ELSEVIER

Materials Science and Engineering A 374 (2004) 292–302

MATERIALS SCIENCE & ENGINEERING A

www.elsevier.com/locate/msea

Crystallography of the B2 → R → B19′ phase transformations in NiTi

Xiangyang Zhang, Huseyin Sehitoglu*

Department of Mechanical and Industrial Engineering, University of Illinois, 1206 W Green Street, Urbana, IL 61801, USA

Received 25 March 2003; received in revised form 25 February 2004

Abstract

The crystallography of B2 to R-phase and the subsequent R-phase to B19′ martensite transitions was analysed in NiTi alloys. Using the energy minimization theory of martensitic transformations, the habit plane and twin plane normals were established for the R-phase, B19′ martensite variants as a function of rhombohedral angle α. Two types of twins, classified as $\{1\,0\,0\}\langle 0\,1\,1\rangle$ and $\{1\,1\,0\}\langle 0\,0\,1\rangle$ compound twins could form in the R-phase. There are 12 R-phase variants with $\{1\,1\,0\}\langle 0\,0\,1\rangle$ compound twins when $\alpha < 90^\circ$. When $\alpha > 90^\circ$ there are 24 R-phase variants with $\{1\,0\,0\}\langle 0\,1\,1\rangle$ compound twins and 12 variants with $\{1\,1\,0\}\langle 0\,0\,1\rangle$ compound twins, respectively. In total, eight possible twins can be formed in B19′ martensite. In the single step B2 to B19′ martensitic transformation, only four twin types are qualified as lattice invariant shear (LIS); while all the eight twin types are qualified as LIS in R-phase to B19′ transition the $\{1\,0\,0\}\langle 0\,1\,1\rangle$ compound, $\{1\,1\,0\}\langle 0\,0\,1\rangle$ compound and $\{1\bar{1}0\}\langle 1\,1\,2.7008\rangle$ Type I twins have been observed in the experiments. The results indicate that the premartensitic R-phase transition plays an important role in understanding the phase transformations in NiTi shape memory alloys.

Keywords: Shape memory; NiTi alloys; R-phase transition; Two-step phase transformations

1. Introduction

The martensitic transformation in NiTi alloys with near-equiatomic compositions has been a focus of extensive research for the last 30 years. The application of these alloys to various fields of engineering and medicine has continued to increase the scientific and technological interest in these materials [1]. The high temperature parent phase of NiTi is a cubic B2, and the lattice of the martensite is a monoclinic B19′ [2–5] phase. The B19′ martensite can be obtained either by a single step transformation of B2 → B19′, or by a two-step transformation of B2 → R-phase → B19′ [6–9]. In the two-step transformation, the R-phase is a rhombohedral phase that is incommensurate with the cubic B2 phase. The lattice parameters of B2 phase, R-phase and B19′ phase, and the lattice correspondences between B2 to R-phase and B2 to B19′ transitions, have been well established [2,3,5,9]. The microstructure of the R-phase was observed as internally twinned and the twin types are $\{1\,1\,0\}_C$ and $\{1\,0\,0\}_C$ compound twins based on the experiments [9–11]. The B19′ martensite was also internal twinned as observed by a number of investigators [3,5,12,13]. A complete analysis of the two stage transformation has not been published in early works.

The eight possible twins predicted by various crystallographic theories of phase transformation are listed in the first column in Table 1 [12,13]. They are designated as Compound-1, Compound-2, Type I-1, Type I-2, Type I-3, Type II-1, Type II-2 and Type II-3 twins respectively in this paper. The experimental observed internal twins of the B19′ martensite reported in early works are $\{1\,1\,\bar{1}\}_M$ Type I, $\{1\,1\,1\}_M$ Type I, $\{0\,1\,1\}_M$ Type I, $\langle 0\,1\,1\rangle_M$ Type II, $(0\,0\,1)_M$ Compound and $(1\,0\,0)_M$ Compound twins [2,3,5,14–17]. They are listed in the second column of Table 1 for comparison with theoretical calculations. The indices of twin elements from theory are in parent B2 lattice and are indicated using the subscript C, while those obtained via experimental measurements are in martensite B19′ lattice and indicated by subscript M. The two coordinate frames are related based on the lattice correspondence relationship between the martensite and the parent phase. From Table 1 we can see that $(1\,0\,0)_M[0\,0\,1]_M$ Compound, $(0\,0\,1)_M[1\,0\,0]_M$ Compound and $(1\,1\,1)_M[\overline{1.5117}\,0.5117\,1]_M$ Type I twins are experimentally observed, but they are not lattice invariant shears (LIS) required by the theories in B2 → B19′ transforma-

* Corresponding author. Tel.: +1-217-333-4112; fax: +1-217-244-6534.
E-mail address: huseyin@uiuc.edu (H. Sehitoglu).

0921-5093/$ – see front matter © 2004 Elsevier B.V. All rights reserved.
doi:10.1016/j.msea.2004.03.013

Table 1
The twins in NiTi B19′ martensite displaying theoretical and experimental values

Possible twins by theory (indexed in parent B2 lattice)	Observed twins in experiments (indexed in martensite B19′ lattice)	Qualified as LIS in B2→B19′ ?
$\{1\,0\,0\}_C\langle 0\,1\,1\rangle_C$ Compound-1	$(1\,0\,0)_M[0\,0\,1]_M$ Compound (ref. [16,17])	No
$\{0\,1\,1\}_C\langle 1\,0\,0\rangle_C$ Compound-2	$(0\,0\,1)_M[1\,0\,0]_M$ Compound (ref. [11,14,16,17])	No
$\{1\,0\,0\}_C\langle 00.7864\,\bar{1}\rangle_C$ Type I-1	$(0\,1\,1)_M[1.57271\bar{1}]]_M$ Type I (ref. [3,14,17])	Yes
$\{1\,\bar{1}\,0\}_C\langle 1\,1\,0.3230\rangle_C$ Type I-2	$(\bar{1}\,\bar{1}\,1)_M[0.5404\,0.4596\,1]_M$ Type I (reference [3,16,17])	Yes
$\{1\,\bar{1}\,0\}_C\langle 1\,1\,2.7008\rangle_C$ Type I-3	$(1\,1\,1)_M[\overline{1.5117}\,0.5117\,1]_M$ Type I (reference [5,15])	No
$\{0.7205\,0\,\bar{1}\}_C\langle 0\,1\,0\rangle_C$ Type II-1	$(0.7205\,1\,\bar{1})_M[0\,1\,1]_M$ Type II (reference [3,15–17])	Yes
$\{\bar{1}\,1\,0.4953\}_C\langle 1\,1\,0\rangle_C$ Type II-2	Not observed	Yes
$\{1\,1\,3.0495\}_C\langle\bar{1}1010\rangle_C$ Type II-3	Not observed	No

Note that compound twins is not qualified as lattice invariant shear (LIS).

tion. Therefore, they were considered as deformation twins in the literature [16,17].

The crystallographic calculation of B2 → B19′ transformation has been the subject of published works in the literature [3,5,12,13]. These calculation include all the possible habit plane variants. In contrast to the B2 → B19′ transformation, the solution for the habit plane normals and deformations for the B2 → R → B19′ transformations have not been satisfactorily completed. A lattice deformation theory calculation of the transformation strains associated with B2 → R transition was provided by Miyazaki and Wayman [9] Miyazaki et al. [10]. The temperature and orientation dependence of transformation strains were determined, but the R-phase was treated as a single crystal in the lattice deformation theory. Therefore deformation results present the 4 lattice correspondence variants of the R-phase, but not the twinned R-phase. A more detailed analysis of the B2 to R-phase transition was conducted recently by Hane and Shield [18]. In this work the microstructure of R-phase and all the possible solutions were obtained. The two studies above have completed the B2 → R-phase transformation only. The first study to undertake the subsequent R → B19′ transformation was published by Krishnan and Singh [11]. In his calculation the R-phase was also treated as a single variant, and the volume fraction ratio of the two lattice correspondence variant in B19′ martensite was assumed as 1:1. This means the major variant within the correspondence variant pair (CVP) and the minor variant have both equal volume fraction. However, in this paper we solve for the twin volume fraction without any assumptions.

A thorough crystallographic solution of B2 → R → B19′ transformations is provided in this work, such as the twin modes, multiple habit plane solutions, using the minimum energy theory of Martensitic transformation [19]. Secondly, we demonstrate that $(1\,0\,0)_M[0\,0\,1]_M$ Compound, $(0\,0\,1)_M[1\,0\,0]_M$ Compound and $(1\,1\,1)_M[\overline{1.5117}\,0.5117\,1]_M$ Type I twins could readily form in the B19′ martensite.

2. The theories of martensitic transformation

The theories of martensitic transformation include the well-known phenomenological theory of Martensite crystallography by Wechsler et al. [20] (known as WLR Theory, 1953) and by Bowles and Mackenzie [21] (known as BM Theory, 1954) and the energy minimization theory by Ball and James [19]. All of these theories are based on the hypothesis that the interface between martensite variant and parent phase is an invariant plane (undeformed and unrotated plane). These theories solve for the orientations of these planes based on the lattice parameters of martensite and parent phase and the lattice correspondence relationship between martensite and parent phase. The phenomenological theory (PT) is based on geometrical and deformation compatibility and the energy minimization theory (EMT) is based on continuum mechanics and free energy minimization and both theories produce equivalent results. The lattice invariant shears are used as input data in PT, while in EMT they are output of the calculation. We use the Energy Minimization Theory in this work and we briefly summarize our calculations for a general case first and then specially for B2 to R-phase and R-phase to B19′ transformations.

A sketch of twinned martensite and parent phase is shown in Fig. 1. The lattice correspondence variants A and B (with

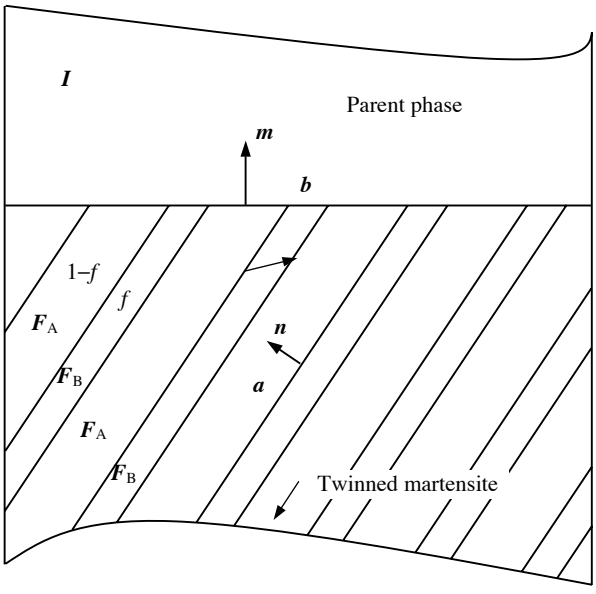

Fig. 1. A sketch of twinned martensite and parent phase.

deformations $\boldsymbol{F}_A$ and $\boldsymbol{F}_B$, respectively) form the twin with a twin plane $\boldsymbol{n}$ and twin shear $\boldsymbol{a}$. The volume fractions of these two variants in a twin are $(1-f)$ and f, respectively. The plane with normal $\boldsymbol{m}$ represents the habit plane between martensite and parent phase, the vector $\boldsymbol{b}$ is the transformation shear and the identity matrix $\boldsymbol{I}$ represents the undeformed parent phase. All these parameters are presented in the parent cubic basis. There are two kinds of invariant planes during martensitic transformation: the interface between the two lattice correspondence variants in the twin and the interface between the twinned martensite and the parent phase. The kinematic compatibility between the two variants across the twin plane requires [19],

$$\boldsymbol{F}_B = \boldsymbol{F}_A + \boldsymbol{a} \otimes \boldsymbol{n} \tag{1}$$

when the twin layers are fine enough, the average deformation of the twinned martensite is given as

$$\boldsymbol{F}_M = \boldsymbol{R}_h[f\boldsymbol{F}_B + (1-f)\boldsymbol{F}_A] \tag{2}$$

where $\boldsymbol{R}_h$ is the relative rotation between twinned martensite and parent phase. So the kinematic compatibility between martensite and parent phase is [19],

$$\boldsymbol{F}_M = \boldsymbol{I} + \boldsymbol{b} \otimes \boldsymbol{m} \tag{3}$$

This equation represents the habit plane strain, the same as those in the phenomenological theories. According to the frame indifference principle in continuum mechanics, Eqs. (1) and (2) can be rewritten as

$$\boldsymbol{R}_{AB}\boldsymbol{U}_B = \boldsymbol{U}_A + \boldsymbol{a} \otimes \boldsymbol{n} \tag{4}$$

$$\boldsymbol{F}_M = \boldsymbol{R}_h[f\boldsymbol{R}_{AB}\boldsymbol{U}_B + (1-f)\boldsymbol{U}_A] \tag{5}$$

where $\boldsymbol{U}_A$ and $\boldsymbol{U}_B$ are the symmetric part of $\boldsymbol{F}_A$ and $\boldsymbol{F}_A$, respectively, based on the polar decomposition $\boldsymbol{F} = \boldsymbol{R}\boldsymbol{U}$ ($\boldsymbol{R}$ is a rotation satisfying $\boldsymbol{R}^T\boldsymbol{R} = \boldsymbol{R}\boldsymbol{R}^T = \boldsymbol{I}$ and $\det \boldsymbol{R} = 1$), $\boldsymbol{R}_{AB}$ the orthogonal tensor and represents the relative rotation between the two variants in the twin. There is no summation for the index B in the equations. The symmetric deformation tensor $\boldsymbol{U}$ uniquely represents the deformation of lattice correspondence variants during martensitic transformation. There are three lattice correspondence variants in cubic to tetragonal, four in cubic to rhombohedral (trigonal), six in cubic to orthorhombic and 12 in cubic to monoclinic transformations [24]. The input for this problem is a lattice correspondence variant pair $\boldsymbol{U}_A$ and $\boldsymbol{U}_B$ and the solution is the quantities of $\boldsymbol{a}$, $\boldsymbol{n}$, $\boldsymbol{b}$, $\boldsymbol{m}$, $\boldsymbol{R}_{AB}$, $\boldsymbol{R}_h$ and f. Details on solving Eqs. (3)–(5) can be found in [12,13,19].

3. One step transformation—B2 to B19′

The B2–B19′ transformation in NiTi alloys have been well investigated utilizing the phenomenological theory [3,5,14] and the Energy Minimization Theory [12,13]. The results are summarized in the following.

Table 2
The lattice correspondence variants (LCVs) for B2–B19′ transformation in NiTi

LCVs	Basis of martensite cell		
	$[1\,0\,0]_m$	$[0\,1\,0]_m$	$[0\,0\,1]_m$
1	$[1\,0\,0]_p$	$[0\,1\,1]_p$	$[0\,\bar{1}\,1]_p$
2	$[\bar{1}\,0\,0]_p$	$[0\,\bar{1}\,\bar{1}]_p$	$[0\,\bar{1}\,1]_p$
3	$[1\,0\,0]_p$	$[0\,\bar{1}\,1]_p$	$[0\,\bar{1}\,\bar{1}]_p$
4	$[\bar{1}\,0\,0]_p$	$[0\,1\,\bar{1}]_p$	$[0\,\bar{1}\,\bar{1}]_p$
5	$[0\,1\,0]_p$	$[1\,0\,1]_p$	$[1\,0\,\bar{1}]_p$
6	$[0\,\bar{1}\,0]_p$	$[\bar{1}\,0\,\bar{1}]_p$	$[1\,0\,\bar{1}]_p$
7	$[0\,1\,0]_p$	$[1\,0\,\bar{1}]_p$	$[\bar{1}\,0\,\bar{1}]_p$
8	$[0\,\bar{1}\,0]_p$	$[\bar{1}\,0\,1]_p$	$[\bar{1}\,0\,\bar{1}]_p$
9	$[0\,0\,1]_p$	$[1\,1\,0]_p$	$[\bar{1}\,1\,0]_p$
10	$[0\,0\,\bar{1}]_p$	$[\bar{1}\,\bar{1}\,0]_p$	$[\bar{1}\,1\,0]_p$
11	$[0\,0\,1]_p$	$[\bar{1}\,1\,0]_p$	$[\bar{1}\,\bar{1}\,0]_p$
12	$[0\,0\,\bar{1}]_p$	$[1\,\bar{1}\,0]_p$	$[\bar{1}\,\bar{1}\,0]_p$

There are 12 lattice correspondence variants in B2 to B19′ transformation as shown in Table 2. The subscript m refers to martensite and p refers to the parent phase. The lattice parameters for the martensite and parent phases are [2,5] $a_0 = 3.15$ Å and $a = 2.889$ Å, $b = 4.120$ Å, $c = 4.622$ Å and $\beta = 96.8^\circ$, respectively. The results of the twin systems and habit planes are listed in Table 3. From the table we can see that the B19′ martensite with Type I-1, Type I-2, Type II-1 and Type II-2 twins can form an invariant plane with parent phase. The dominantly observed twin in near-equiatomic NiTi is the Type II-1 twin [12,13]. In previous work we have presented the resolved shear stress factor (RSSFs) and the transformation strains for Type II-1 twinning [13].

4. Two step transformation—B2 to R-phase and R-phase to B19′

The two step transformations of B2 → R-phase and subsequent R-phase → $B19'$ may occur upon cooling when R_s (the start temperature of B2 → R-phase transition) is above M_s (start temperature of martensite transformation) [6,25]. This phenomenon was also observed in stress-induced transformations [7–10]. The differential scanning calorimeter (DSC) curve and the stress–strain curve [26] in Fig. 2a and b show the temperature-induced and stress-induced two-step transitions in an alloy of NiTi, respectively. Upon cooling the parent phase B2 transfers to rhombohedral phase (R-phase) at R_s, R-phase to martensitic phase at M_s, and the martensitic transformation from R-phase is completed at M_f. The reverse transformation occurs from martensitic phase directly to the parent phase B2 at A_s and is completed at A_f.

Fig. 3 illustrates the two-step transformation schematically and the unit cells of each phase are also shown. The austenite is denoted as B2 with cubic unit cell and the lattice axes are $\boldsymbol{a}$, $\boldsymbol{b}$ and $\boldsymbol{c}$, respectively. The unit cell of rhombohedral phase is created from the B2 cell by elongating the

Table 3
Summary of crystallographic solutions of B2 to B19′ transformation in NiTi

Twin systems	Correspondence variant pairs (CVPs)	Volume fraction	Habit planes
Compound-1	(1,2), (3,4), (5,6), (7,8), (9,10), (11,12)	None	None
Compound-2		None	None
Type I-1	(1,3), (1,4), (2,3), (2,4), (5,7), (5,8), (6,7), (6,8), (9,11), (9,12), (10,11), (10,12)	$f = 0.292$	$(\boldsymbol{m}, \boldsymbol{b}) = (\{0.9087,0.3333,0.2513\}, \langle 0.2527,0.0535,0.1060\rangle)$ $(\boldsymbol{m}, \boldsymbol{b}) = (\{0.3464,0.4333,0.8320\}, \langle 0.1210,0.0397,0.0256\rangle)$
Type II-1		$f = 0.271$	$(\boldsymbol{m}, \boldsymbol{b}) = (\{0.8138,0.0009,0.5811\},\langle 0.0350,0.0934,0.0433\rangle)$ $(\boldsymbol{m}, \boldsymbol{b}) = (\{0.2779,0.8589,0.4301\},\langle 0.0901,0.0052,0.0606\rangle)$
Type I-2	(1,5), (1,9), (2,7), (2,12), (3,6), (3,11), (4,8), (4,10), (5,9), (6,11), (7,12), (8,10)	$f = 0.320$	$(\boldsymbol{m}, \boldsymbol{b}) = (\{0.8887,0.0418,0.4565\},\langle 0.0278,0.1008,0.0375\rangle)$ $(\boldsymbol{m}, \boldsymbol{b}) = (\{0.2012,0.9099,0.3628\},\langle 0.0999,0.0010,0.0484\rangle)$
Type II-2		$f = 0.323$	$(\boldsymbol{m}, \boldsymbol{b}) = (\{0.8889,0.4044,0.2152\},\langle 0.0568,0.0637,0.0991\rangle)$ $(\boldsymbol{m}, \boldsymbol{b}) = (\{0.3762,0.5136,0.7712\},\langle 0.1195,0.0485,0.0216\rangle)$
Type I-3	(1,8), (1,11), (2,6), (2,10), (3,7), (3,9),	None	None
Type II-3	(4,5), (4,12), (5,12), (6,10), (7,9), (8,11)	None	None

latter along any one of the ⟨1 1 1⟩ directions [10]. The lattice axes of R-phase unit are $\boldsymbol{a}'$, $\boldsymbol{b}'$ and $\boldsymbol{c}'$, respectively. The α is known as rhombohedral angle which is temperature dependent and changes during cooling [6,10,22]. The unit cell of B19' phase is not shown here and can be found in [16,17]. The R-phase is internally twinned with a twin plane normal $\boldsymbol{n}_1$ and twin shear vector $\boldsymbol{a}_1$. The relative volume fractions of the two lattice correspondence variants in the twin are f_1 and $1-f_1$, respectively. The R-phase has a habit plane $\boldsymbol{m}_1$ with the parent phase. The transformation direction from B2 to R-phase is denoted as $\boldsymbol{b}_1$. Note that $\boldsymbol{b}_1$ is not a unit vector and includes the transformation magnitude. The subsequent B19′ martensite is also twinned with a twin plane normal $\boldsymbol{n}_2$ and a twin shear vector $\boldsymbol{a}_1$, and the volume fractions of the two variants in the twin are f_2 and $1-f_2$, respectively. The habit plane between R-phase and B19′ martensite is denoted as $\boldsymbol{m}_2$ and the corresponding transformation direction is $\boldsymbol{b}_2$. The twin systems and habit planes associated with this two-step transition are calculated in the following sections by using the energy minimization theory.

4.1. B2 to R-phase transition

There are four lattice correspondence variants in B2 to R-phase transition according to the lattice relationship as shown in Fig. 3. Assuming that the length of the sides of cubic and trigonal unit cells is same, the transition can be solely described by the rhombohedral angle α and the deformation matrices in B2 coordinates are [9,10,23].

$$U_1 = \begin{bmatrix} \eta & \delta & \delta \\ \delta & \eta & \delta \\ \delta & \delta & \eta \end{bmatrix}, \quad U_2 = \begin{bmatrix} \eta & -\delta & \delta \\ -\delta & \eta & -\delta \\ \delta & -\delta & \eta \end{bmatrix},$$

$$U_3 = \begin{bmatrix} \eta & \delta & -\delta \\ \delta & \eta & -\delta \\ -\delta & -\delta & \eta \end{bmatrix}, \quad U_4 = \begin{bmatrix} \eta & -\delta & -\delta \\ -\delta & \eta & \delta \\ -\delta & \delta & \eta \end{bmatrix}$$

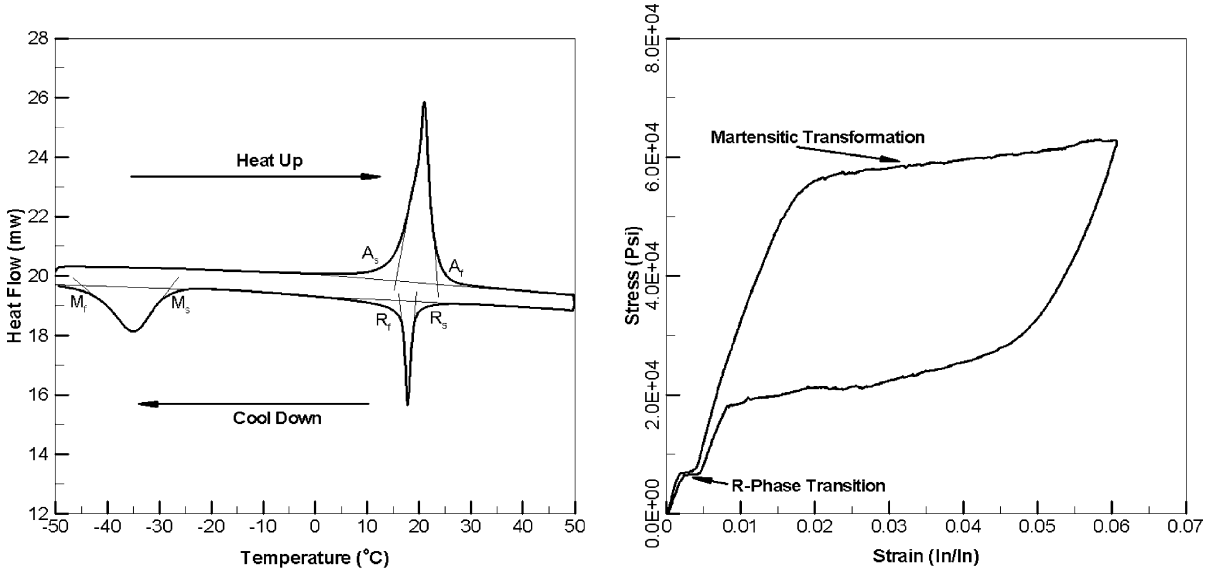

(a) DSC Curve (b) Stress-Strain Cure

Fig. 2. Evidence of two-step transition in an aged NiTi alloy [26].

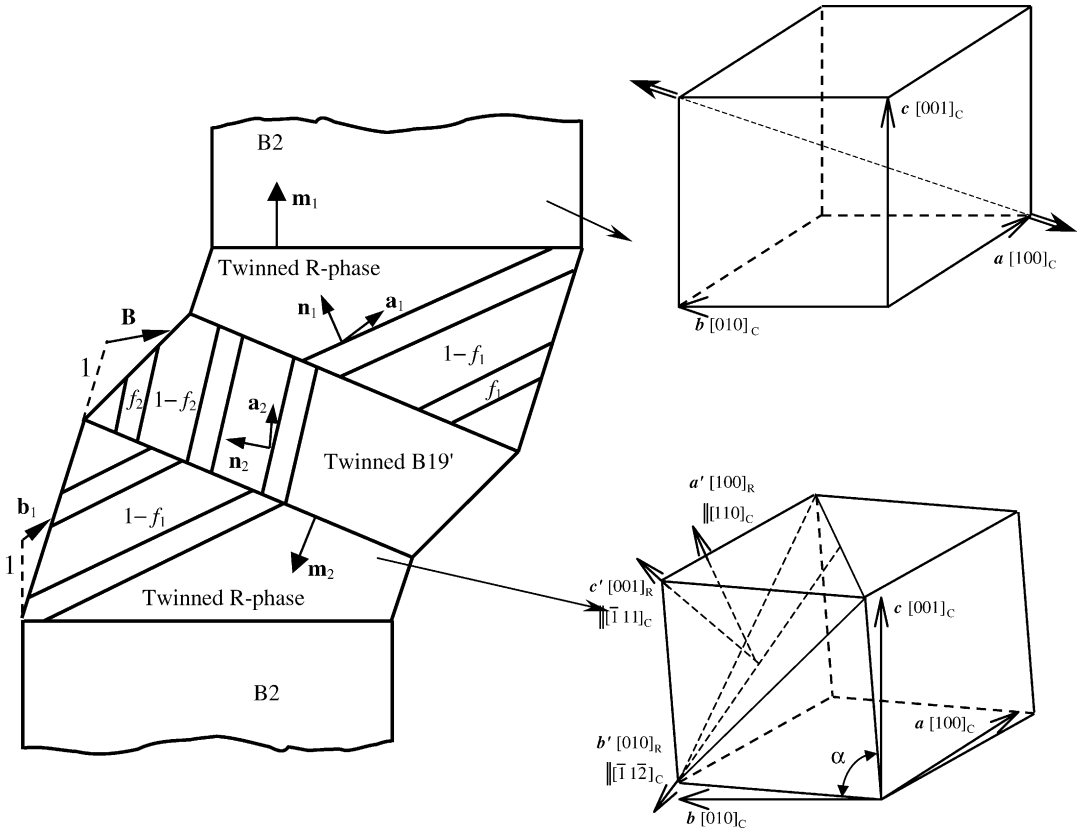

Fig. 3. A schematic showing the transformation planes and directions associated with successive step transformation of B2 → *R*-phase and R-phase → B19′ and the unit cells of B2 phase and rhombohedral phase.

where $\eta = (\sqrt{1+2\cos\alpha} + 2\sqrt{1-\cos\alpha})/3$ and $\delta = (\sqrt{1+2\cos\alpha} - \sqrt{1-\cos\alpha})/3$.There are six variants pairs which can form twins in R-phase, e.g., (1,2), (1,3), (1,4), (2,3), (2,4) and (3,4). Substituting any pair of variants into Eq. (4), the twin planes $\boldsymbol{a}_1$ and twin shears $\boldsymbol{n}_1$ are obtained. The $\{1\,0\,0\}_C\langle 0\,1\,1\rangle_C$ and $\{1\,1\,0\}_C\langle 0\,0\,1\rangle_C$ compound twins are possible for any of the pairs no matter what the rhombohedral angle α. These twins have also been observed in the experiments [9]. Substituting $\boldsymbol{a}_1$ and $\boldsymbol{n}_1$ into Eqs. (3) and (5), the habit plane orientations $\boldsymbol{m}_1$, the transformation shears $\boldsymbol{b}_1$ and the volume fraction f_1 can be calculated. The results are shown in Table 4 for some selected rhombohedral angles. The habit plane variants with the $\{1\,0\,0\}_C\langle 0\,1\,1\rangle_C$ compound twin only exist when $\alpha > 90^\circ$; while the habit plane variants with the $\{1\,1\,0\}_C\langle 0\,0\,1\rangle_C$ compound twin exist for both $\alpha > 90^\circ$ and $<90^\circ$. There are 24 habit plane variants with $\{1\,1\,0\}_C\langle 0\,0\,1\rangle_C$ Compound twin and 24 with $\{1\,0\,0\}_C\langle 0\,1\,1\rangle_C$ compound twin. The two lattice correspondence variants in $\{1\,1\,0\}_C\langle 0\,0\,1\rangle_C$ compound twin have the same volume fraction of 0.5, while the volume fraction of the two variants in $\{1\,0\,0\}_C\langle 0\,1\,1\rangle_C$ compound twin varies with α.

Once the habit plane orientations and transformation shears are determined, it is possible to establish the trans-

Table 4
Summary of the calculation of B2 to R-phase transition

Twin system		$\{1\,0\,0\}_C\langle 0\,1\,1\rangle_C$ Compound	$\{1\,1\,0\}_C\langle 0\,0\,1\rangle_C$ Compound
Range of α with solutions		$\alpha > 90^\circ$	Both $\alpha > 90^\circ$ and $<90^\circ$
Number of solutions		24	24 (12 independent)
Examples of solution	$\alpha = 87.0^\circ$	No solution	$f_1 = 0.5$, $\boldsymbol{m}_1 = \{0, 0.0276, 0.9996\}$ $\boldsymbol{b}_1 = \langle 0, 0.0496, 0.0026\rangle$
	$\alpha = 88.5^\circ$	No solution	$f_1 = 0.5$, $\boldsymbol{m}_1 = \{0, 0.0134, 0.9999\}$ $\boldsymbol{b}_1 = \langle 0, 0.0255, 0.0007\rangle$
	$\alpha = 91.5^\circ$	$f_1 = 0.4191$, $\boldsymbol{m}_1 = \{0.0, 0.1597, 0.9872\}$ $\boldsymbol{b}_1 = \langle 0.0265, 0.0043, 0.0004\rangle$	$f_1 = 0.5$, $\boldsymbol{m}_1 = \{0, 0.0128, 0.9999\}$ $\boldsymbol{b}_1 = \langle 0, 0.0269, 0.0007\rangle$
	$\alpha = 93.0^\circ$	$f_1 = 0.3856$, $\boldsymbol{m}_1 = \{0.0, 0.2230, 0.9784\}$ $\boldsymbol{b}_1 = \langle 0.0537, 0.1263, 0.0015\rangle$	$f_1 = 0.5$, $\boldsymbol{m}_1 = \{0, 0.0249, 0.9997\}$ $\boldsymbol{b}_1 = \langle 0, 0.0551, 0.0029\rangle$

formation strain as:

$$\varepsilon_1 = \tfrac{1}{2}(\boldsymbol{F}_1^T \boldsymbol{F}_1 - \boldsymbol{I}) = \tfrac{1}{2}[\boldsymbol{b}_1 \otimes \boldsymbol{m}_1 + \boldsymbol{m}_1 \otimes \boldsymbol{b}_1 + (\boldsymbol{b}_1 \boldsymbol{b}_1)\boldsymbol{m}_1 \otimes \boldsymbol{m}_1] \quad (6)$$

where

$$\boldsymbol{F}_1 = \boldsymbol{I} + \boldsymbol{b}_1 \otimes \boldsymbol{m}_1 \quad (7)$$

Under a certain uniaxial loading with loading direction $\boldsymbol{e}$, the deformation along the loading direction is then given by

$$E_1 = \boldsymbol{e}\varepsilon_1\boldsymbol{e} = (\boldsymbol{e}\boldsymbol{b}_1)(\boldsymbol{m}_1\boldsymbol{e}) + \tfrac{1}{2}(\boldsymbol{b}_1\boldsymbol{b}_1)(\boldsymbol{e}\boldsymbol{m}_1)^2 \quad (8)$$

The orientation dependence of the transformation strain can be calculated by using Eq. (8). The transformation strains are also related to the rhombohedral angle α. As an example, Fig. 4a and b shows the equivalent transformation strain contours on a standard $(0\,0\,1)_C$ stereographic triangle when $\alpha = 91.5°$. From Fig. 4a and b we note that for $\{1\,1\,0\}_C\langle 0\,0\,1\rangle_C$ compound twinned variants the minimum value appears in the $\langle 0\,0\,1\rangle_C$ orientation and maximum in $\langle 0\,1\,1\rangle_C$ orientation; while for $\{1\,0\,0\}_C\langle 0\,1\,1\rangle_C$ compound twinned variants the minimum appears in $\langle 0\,0\,1\rangle_C$ under tension (Fig. 4a) and in $\langle 1\,3\,3\rangle_C$ orientation under compression (Fig. 4b).

The transformation strains change continuously with the variation of α. We present results of transformation strains for some selected orientations ($\langle 0\,0\,1\rangle_C$, $\langle 0\,1\,1\rangle_C$, $\langle 1\,1\,1\rangle_C$ and $\langle 1\,1\,2\rangle_C$) and different angles α in Fig. 5a and b. In Fig. 5a and b the dashed lines represent the results of $\{1\,0\,0\}_C\langle 0\,1\,1\rangle_C$ compound twinned variants which

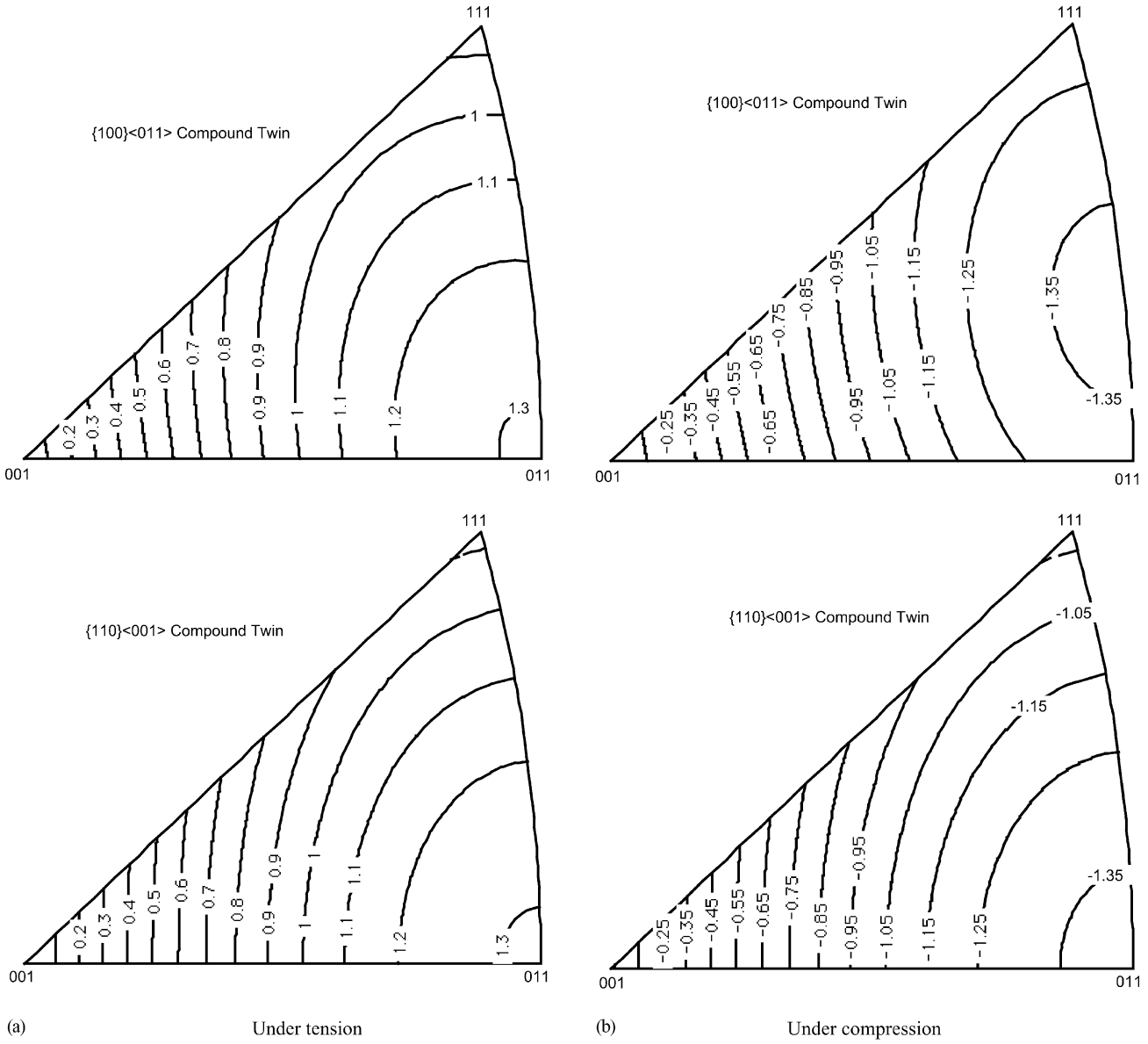

(a) Under tension (b) Under compression

Fig. 4. Equivalent transformation strain contour associated with B2 to R-phase transition (from Eq. (8)) for the two different twin types when $\alpha = 91.5°$.

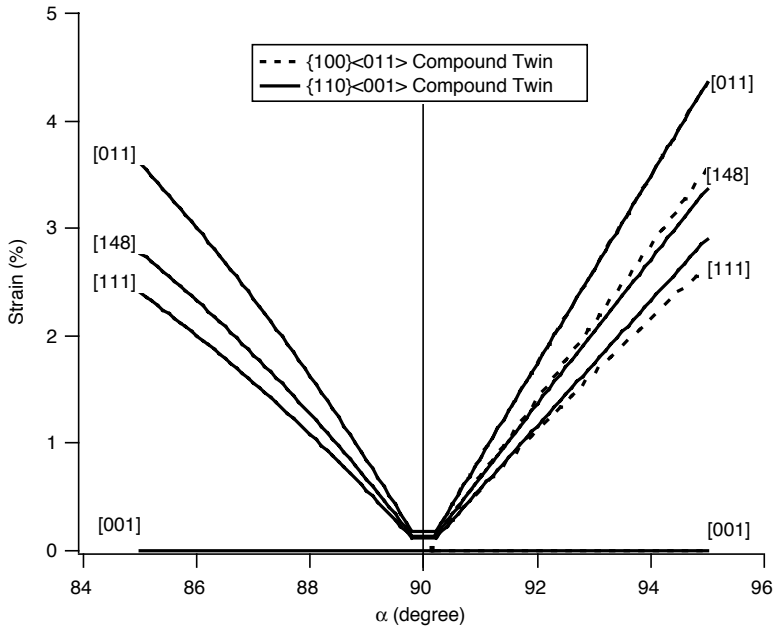

(a) Under tension

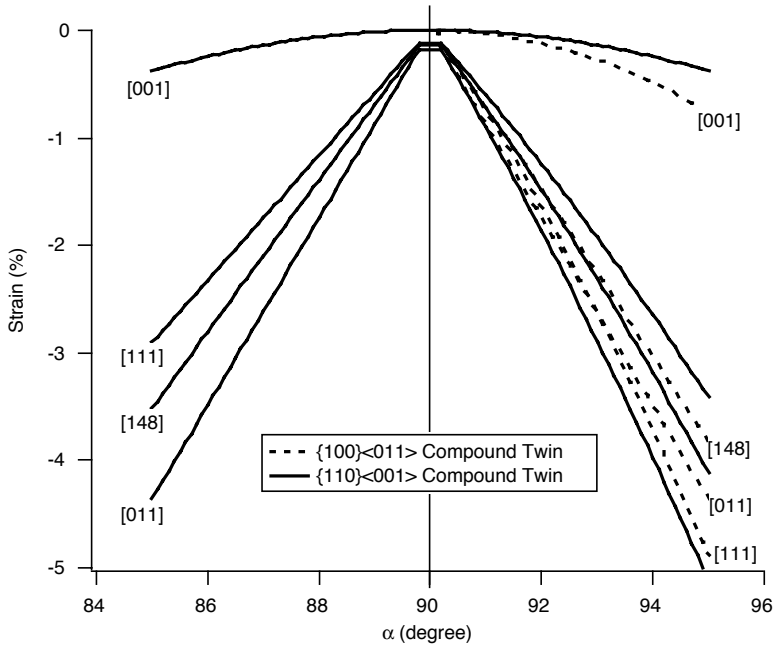

(b) Under compression

Fig. 5. Calculated α-dependence of the transformation strains of B2 to R-phase transition for various orientations.

only exist in the range of $\alpha > 90^\circ$ and the solid lines are those of $\{1\,1\,0\}_C\langle 0\,0\,1\rangle_C$ compound twinned variants. The transformation strains in $\langle 0\,1\,1\rangle_C$ and $\langle 0\,0\,1\rangle_C$ orientation under tension are same for both $\{1\,0\,0\}_C\langle 0\,1\,1\rangle_C$ compound twinned variants and the $\{1\,1\,0\}_C\langle 0\,0\,1\rangle_C$ compound twinned variants. The strains in $\langle 0\,0\,1\rangle_C$ direction are zero under tension for all variants.

4.2. R-phase to B19′

We now consider the second stage of transformation. Since both the B19′ variants from one step transformation and from two-step transformation have the same lattice structure, they have the same lattice correspondence with the B2 phase. The possible twins in B19′ martensite are deter-

mined by Eq. (4) and are the same as those listed in Table 2. The habit plane orientations and the transformation shears are determined by

$$\boldsymbol{F}_2 - \boldsymbol{F}_1 = \boldsymbol{b}_2 \otimes \boldsymbol{m}_2 \tag{9}$$

where $\boldsymbol{F}_1$ is the average deformation of R-phase calculated by Eq. (7) when $\boldsymbol{m}_1$ and $\boldsymbol{b}_1$ are known, and $\boldsymbol{F}_2$ is the average deformation of twinned B19′ determined as

$$\boldsymbol{F}_2 = \boldsymbol{R}_\mathrm{h}(\boldsymbol{U}_i + f_2 \boldsymbol{a}_2 \otimes \boldsymbol{n}_2) \tag{10}$$

Using one twinned R-phase as matrix and substituting Eq. (10) into Eq. (9), the solutions of $\boldsymbol{R}_\mathrm{h}, f_2, \boldsymbol{b}_2$ and $\boldsymbol{m}_2$ are obtained.

Two factors will influence the solutions for the active habit plane variants and transformation strains. The first factor hinged upon which R-phase variant is selected as matrix. From the results of B2 to R-phase transition in Section 4.1, there are 12 R-phase variants with $\{1\,1\,0\}_\mathrm{C}\langle 0\,0\,1\rangle_\mathrm{C}$ compound twin when $\alpha\langle 90^\mathrm{o}$ and 12 variants with $\{1\,1\,0\}_\mathrm{C}\langle 0\,0\,1\rangle_\mathrm{C}$ and 24 variants with $\{1\,0\,0\}_\mathrm{C}\langle 0\,1\,1\rangle_\mathrm{C}$ compound twins when $\alpha > 90^\circ$. Using different R-phase variants will result in different B19′ martensite variants. We use an algorithm in the calculation such that under a particular direction of uniaxial loading, we select the most favorable R-phase variant according to the maximum RSSF, and then use this R-phase variant as the matrix in Eq. (9) to calculate all the possible B19′ martensite variants. Similarly the most favorable B19′ variant under the same direction of load is selected using the RSSF criterion. Therefore, the orientation dependence of B19′ martensite is established. In the calculation we treat $\{1\,0\,0\}_\mathrm{C}\langle 0\,1\,1\rangle_\mathrm{C}$ and $\{1\,1\,0\}_\mathrm{C}\langle 0\,0\,1\rangle_\mathrm{C}$ compound twinned R-phase variants separately. That is, the most favorable R-phase variant is selected within the 24 R-phase variants with $\{1\,0\,0\}\langle 0\,1\,1\rangle$ compound twin or within the 12 variants with $\{1\,1\,0\}\langle 0\,0\,1\rangle$ compound twin separately.

The second factor that influences the active habit planes and transformation strains is the rhombohedral angle, α, of the R-phase. The results in Section 4.1 show that different α produces different R-phase variants, and naturally this results in different B19′ martensite variants. As we have known Type I-1, Type I-2, Type II-1 and Type II-2 twins serve as LIS in the single step B2 to B19′ martensite transformation, while Compound-1, Compound-2, Type I-3 and Type II-3 twins are not the LIS in single step phase transformation. In the two-step transformation, Type I-1, Type I-2, Type II-1 and Type II-2 twins are still the LIS in B19′ martensite. Besides these four types of twin, Compound-1, Compound-2, Type I-3 and Type II-3 twins are found to be lattice invariant shear when α has special values. Using R-phase variant with $\{1\,1\,0\}_\mathrm{C}\langle 0\,0\,1\rangle_\mathrm{C}$ compound twin as matrix, the solutions of B19′ variants with Type I-3 and Type II-3 twins are obtained when $\alpha < 86.0^\circ$ or $\alpha > 93.7^\circ$. Using R-phase variants with $\{1\,0\,0\}_\mathrm{C}\langle 0\,1\,1\rangle_\mathrm{C}$ compound twin as matrix, B19′ variants with Type I-3 and Type II-3 twins are obtained when $\alpha > 93.7^\circ$, and B19′ variants with Compound-1 and Compound-2 twins are obtained when $93.9^\circ < \alpha < 95.1^\circ$. Therefore, all the eight types of twin listed in the first column in Table 1 could serve as lattice invariant shear in R-phase to B19′ martensitic transformation.

The habit plane orientations and transformation shears of the B19′ variants with Type I-1, Type I-2, Type II-1 and Type II-2 twins are different depending on α. The orientation dependence of the total transformation strains (the strains associated with B2 → R-phase → B19′ martensite) are shown in Fig. 6 for three different rhombohedral angle $\alpha = 88.5$, 90.0 and 91.5°. The result of $\alpha = 90.0^\circ$ equals to that of single step transformation. Fig. 7 shows the total transformation strains for several selected directions. The strains in Figs. 6 and 7 are calculated from B2 to $\{1\,1\,0\}_\mathrm{C}\langle 0\,0\,1\rangle_\mathrm{C}$ compound twinned R-phase and further to B19′ martensite. The B19′ martensite considered here is in Type II-1 twinned. The strains associated with $B2 \rightarrow \{1\,0\,0\}_C\langle 0\,1\,1\rangle_C$ compound twinned R-phase → $B19'$ martensite are similar, therefore they are not shown here. The curves under compression demonstrate that the single step and two-step transformations have similar deformation levels except in the [1 1 1] orientation. The strains increase with the increase of $|\alpha - 90^\circ|$ for the two-step transformation under tension. Only in [0 0 1] direction the strain is maintained the same since in this direction the strain associated with B2 to R-phase transition is zero (refer to Fig. 4a). In single step transformation, the habit plane is the interface between B19′ martensite and parent phase, and the habit plane orientations and transformation shears are fixed. While in two-step transformation, the habit plane is the interface between B19′ martensite and R-phase, and both the habit plane orientations and transformation shears vary with α, as well as the relative volume fraction of the two lattice correspondence variants in the twin.

The new habit plane variants with Compound-1, Compound-2, Type I-3 and Type II-3 twins are obtained in the two-step transformations when α is in a certain range. As we can see in the second column of Table 1, Compound-1, Compound-2 and Type I-3 twins have been observed in the experiments in NiTi alloys. These twins were classified as deformation twins (caused by elastic interactions among martensitic plates) which differ than lattice invariant shear since they cannot provide a habit plane solution to the crystallographic theory of martensitic transformation [16,17,27]. Our calculation shows that it is possible for the compound twins to serve as lattice invariant shear in the R-phase to B19′ transition.

A recent study by Krishnan and Singh [11] confirmed the existence of B19′ martensite with Compound-2 twin and gave explanations on how this twin forms and why the Compound-2 twinned B19′ martensite variant is preferred. The R-phase to B19′ transition was calculated in [11], but the results are not the same as ours. The differences exist in the following four aspects:

(1) The case that a single crystal of R-phase transfers to B19′ martensite was considered in [11], while in our

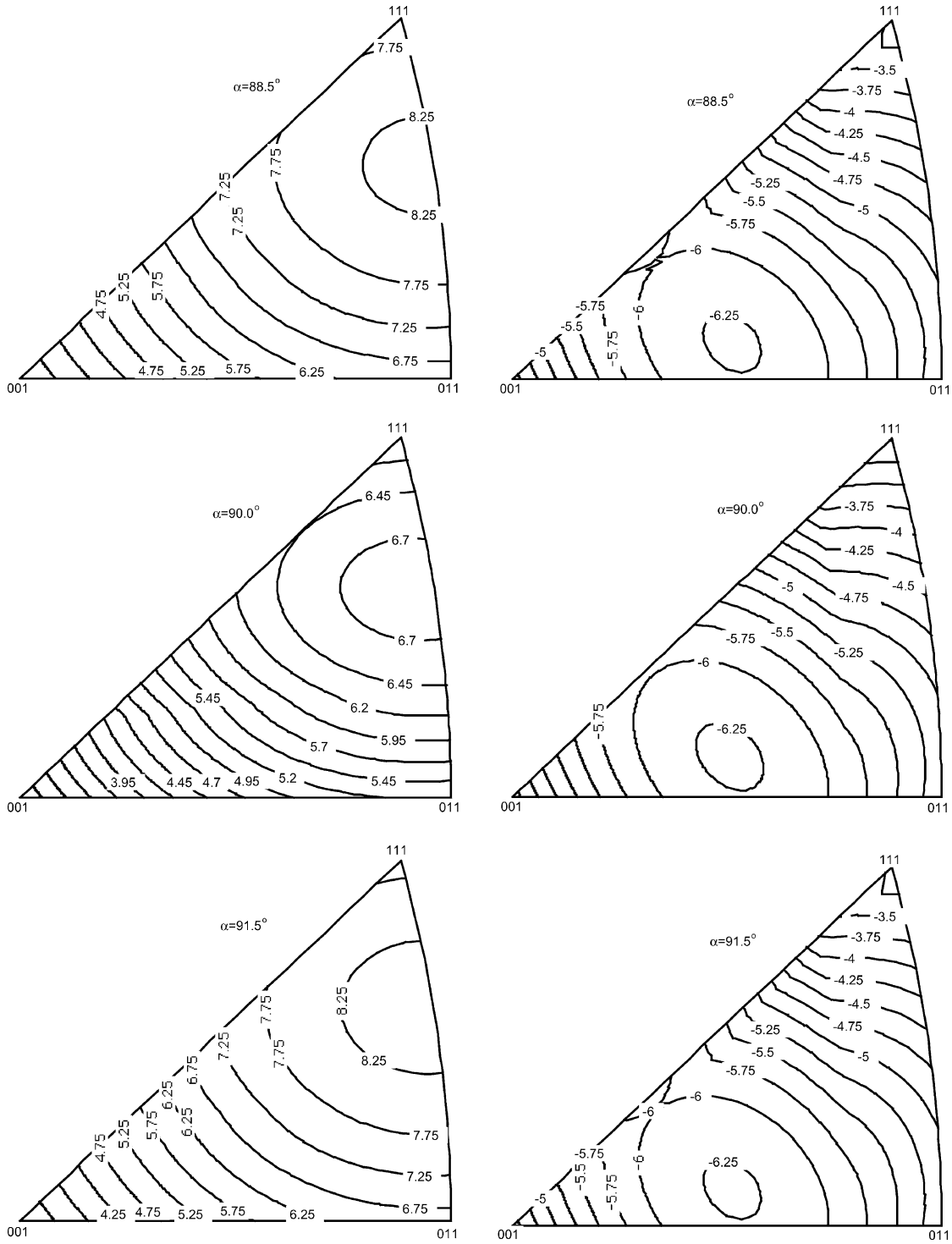

(a) Under tension

(b) Under compression

Fig. 6. Equivalent B2 → R-phase → Type II-1 B19′ martensitic transformation strain contour when $\alpha = 88.5$, 90.0 and 91.5°.

study the B19′ martensite is produced from a twinned R-phase. The deformation of a single crystal R-phase is one of the four matrices $\boldsymbol{U}_1, \boldsymbol{U}_2, \boldsymbol{U}_3$ and $\boldsymbol{U}_4$ as shown in Section 4.1, and the deformation of a twinned R-phase is one of 36 (24 with $\{1\,0\,0\}\langle 0\,1\,1\rangle$ Compound twin and 12 with $\{1\,1\,0\}\langle 0\,0\,1\rangle$ Compound twin) $\boldsymbol{F}_1$ calculated by Eq. (7).

(2) Only the results of R-phase to Compound-2 twinned B19′ martensitic transformation was calculated in [11], while in our study all the possible twin types were con-

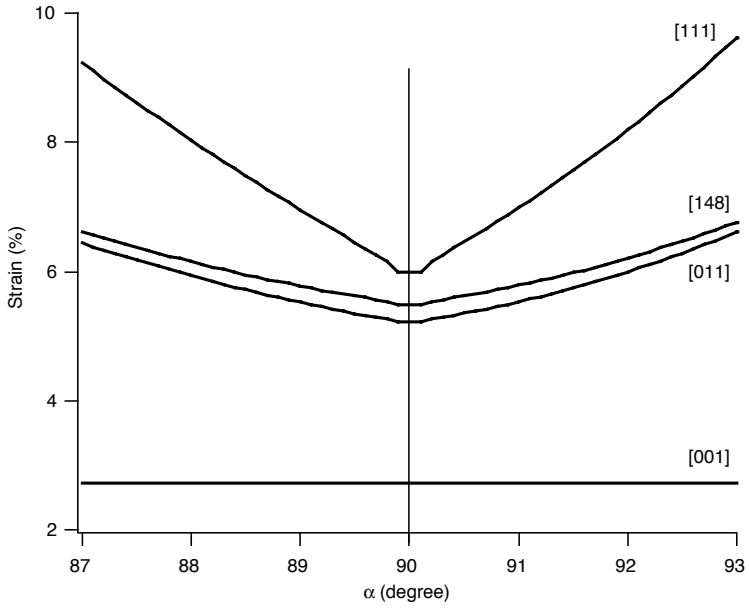

(a) Under tension

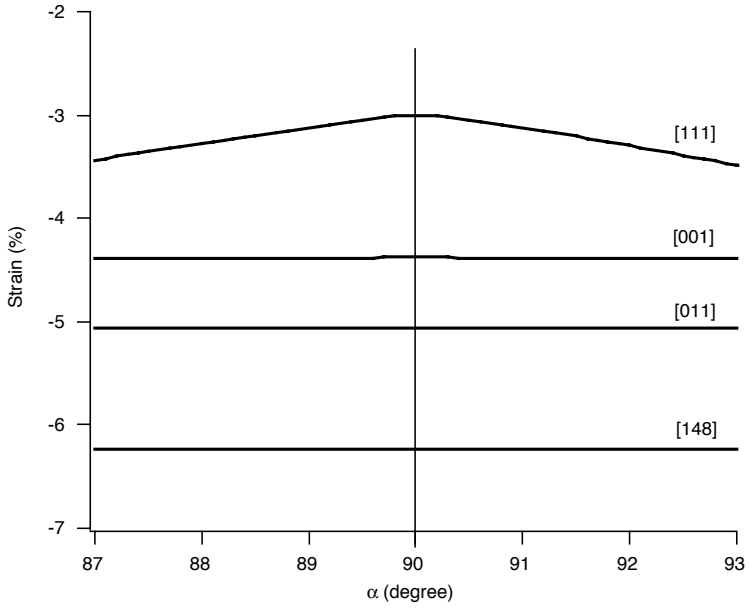

(b) Under compression

Fig. 7. Calculated α-dependence of the total two-step transformation strains of Type II-1 B19′ variants for various orientations.

sidered and all of the possible habit plane variants were presented.

(3) The volume fraction of the major variant and minor variant in B19′ martensite was fixed as 1:1 in [11], while in our study the data is the output of the calculation and changes with the variation of rhombohedral angle α.

(4) The B19′ martensite with Compound-2 twin only exists when the rhombohedral angle α equals to a critical value 86.2° in [11], in our study the rhombohedral α is in the range 85–95.1°. Preliminary results for the 94.1° were given in [28].

5. Conclusions

The following conclusions are drawn in this study:

(1) A complete calculation of B2 to R-phase transition is provided. There are 24 $\{1\,1\,0\}_C\langle 0\,0\,1\rangle_C$ twinned R-phase variants when $\alpha < 90°$ and 24 $\{1\,1\,0\}_C\langle 0\,0\,1\rangle_C$ and 24 $\{1\,0\,0\}_C\langle 0\,1\,1\rangle_C$ twined R-phase variants when $\alpha > 90°$. Within the 24 variants with $\{1\,1\,0\}_C\langle 0\,0\,1\}_C$ twins, twelve of them are independent because the volume ratio of the two lattice correspondence variants in

the twin is always in half. The transformation strains associated with B2 to R-phase transition increase with the increase of $|\alpha - 90^\circ|$. One exception is that the strain remains zero under tension load in $\langle 0\,0\,1\rangle_C$ direction.

(2) The subsequent transition of twinned R-phase to twinned B19′ martensite is studied in detail. A variety of possible B19′ martensite variants are obtained by using different twinned R-phase as matrix and by changing the rhombohedral angle α. The orientation dependence of the total transformation strain is determined when the maximum resolved shear stress is used as variant selection criterion. The results show that the total transformation strain associated with B2 to R-phase to B19′ transition is insensitive to α under compression, while under tension it is sensitive to α. The total transformation strains increase with the increase of $|\alpha - 90^\circ|$ under tension, while under compression the transformation strains of two-step transformation keep similar with those of single step transformation. The exception is again in $\langle 0\,0\,1\rangle_C$ direction, the strain keeps zero under tension and increases with increase of $|\alpha - 90^\circ|$ under compression. The B19′ martensite variants with four new types of twin, which do not exist in B2 to B19′ single step transformation (i.e. $\alpha = 90^\circ$), are found in the two-step transitions. The B19′ variants with Type I-3 and Type II-3 twins are obtained when they are transferred from $\{1\,1\,0\}_C\langle 0\,0\,1\rangle_C$ twinned R-phase and when $\alpha < 86.0^\circ$ or $\alpha > 93.7^\circ$. These variants are also obtained when they are transferred from $\{1\,0\,0\}_C\langle 0\,1\,1\rangle_C$ twinned R-phase and $\alpha > 93.7^\circ$. The B19′ variants with Compound-1 and Compound-2 twins are obtained when they are transferred from $\{1\,0\,0\}_C\langle 0\,0\,1\rangle_C$ twinned R-phase and when $93.9^\circ < \alpha < 95.1^\circ$.

(3) $\{1\,1\,0\}_C\langle 0\,0\,1\rangle_C$ and $\{1\,0\,0\}_C\langle 0\,1\,1\rangle_C$compound twins and $\{1\,\bar{1}\,0\}_C\langle 1\,1\,0.3230\rangle_C$ Type I twin were experimental observed in NiTi alloys, but they are not lattice invariant shears in B2 to B19′ transformation. In this study they are found to be LIS in R-phase to B19′ transformation.

Acknowledgements

The research is supported partially by the National Science Foundation, CMS 99-00090, Mechanics and Materials Program, Arlington, Virginia, and the Air Force Office of Scientific Research, Arlington, Virginia.

References

[1] K. Otsuka, C.M. Wayman (Eds.), Shape Memory Materials, Cambridge University Press, Cambridge, 1998.
[2] K. Otsuka, T. Sawamura, K. Shimuzu, Phys. Stat. Sol. 5a (1971) 457–470.
[3] K.M. Knowles, D.A. Smith, Acta Metall. Mater. 29 (1) (1981) 101–110.
[4] S. Miyazaki, S. Kimura, K. Otsuka, Y. Suzuki, Scripta Metall. 18 (1984) 883–888.
[5] O. Matsumoto, S. Miyazaki, K. Otsuka, H. Tamura, Acta Metall. Mater. 35 (8) (1987) 2137–2144.
[6] H.C. Ling, R. Kaplow, Mater. Sci. Eng. 51 (1981) 193–201.
[7] C.M. Huang, M.E. Meichle, M.B. Salamon, C.M. Wayman, Philosophical Mag. 47A (1983) 31.
[8] M.B. Salamon, M.E. Meichle, C.M. Wayman, Phys. Rev. 31B (1985) 7306.
[9] S. Miyazaki, C.M. Wayman, Acta Metall. Mater. 36 (1) (1988) 181–192.
[10] S. Miyazaki, S. Kimura, K. Otsuka, Philosophical Mag. 57A (3) (1988) 467–478.
[11] M. Krishnan, J.B. Singh, Acta Mater. 48 (6) (2000) 1325–1344.
[12] K.F. Hane, T.W. Shield, Acta Mater. 47 (9) (1999) 2603–2617.
[13] H. Sehitoglu, I. Karaman, R. Anderson, X. Zhang, K. Gall, H.J. Maier, Y. Chumlyakov, Acta Mater. 48 (10) (2000) 3311–3326.
[14] S.P. Gupta, A.A. Johnson, Tans. JIM 14 (1973) 292–302.
[15] Y. Kudoh, M. Tokonami, S. Miyazaki, K. Otsuka, Acta Metall. Mater. 33 (11) (1985) 2049–2056.
[16] T. Onda, Y. Bando, T. Ohba, K. Otsuka, Mater. Trans. JIM 33 (4) (1992) 354–359.
[17] M. Nishida, H. Ohgi, I. Itai, A. Chiba, K. Yamauchi, Acta Metall. Mater. 43 (3) (1995) 1219–1227.
[18] K.F. Hane, T.W. Shield, Mater. Sci. Eng. A291 (2000) 147–159.
[19] J.M. Ball, R.D. James, Arch. Rat. Mech. Anal. 100 (1987) 13–52.
[20] M.S. Wechsler, D.S. Lieberman, T.A. Read, Trans. AIME 197 (1953) 1503–1515.
[21] J.S. Bowles, J.K. Mackenzie, Acta Metall. 2 (1954) 129.
[22] Q.P. Sun, X.Y. Zhang, T.T. Xu, ASME J. Eng. Mater. Technol. 121 (1) (1999) 38–43.
[23] X.Y. Zhang, Q.P. Sun, S.W. Yu, J. Mech. Phys. Solids 48 (10) (2000) 2163–2182.
[24] R.D. James, K.F. Hane, Acta Mater. 48 (1) (2000) 197–222.
[25] H.C. Ling, R. Kaplow, Metall. Trans. 11A (1) (1980) 77–83.
[26] X.Y. Zhang, Internal Report, Edwards Lifesciences, 2002.
[27] M. Nishida, K. Yamauchi, I. Itai, H. Ohgi, A. Chiba, Acta Metall. Mater. 43 (3) (1995) 1229–1234.
[28] H. Sehitoglu, J. Jun, X. Zhang, I. Karaman, Y. Chumlyakov, H.J. Maier, K. Gall, Acta Mater. 49 (2001) 3609–3620.